tektonika



# Practical Assessment of Quartz Crystallographic Preferred Orientation Strength

**Kyle P. Larson** *[1], **Riccardo Graziani** [1,2], **Rüdiger Kilian** [3], **Nicolas Piette-Lauzière** [1]

[1]Department of Earth, Environmental and Geographic Sciences, University of British Columbia Okanagan, 3247 University Way, Kelowna, BC, Canada, V1V 1V7 | [2]Geological Survey of Canada, 601 Booth Street, Ottawa ON, Canada, K1A 0E8 | [3]Institute of Geosciences and Geography, Martin Luther University Halle-Wittenberg, von-Seckendorff-Platz 3, 06120 Halle, Germany

**Abstract** The ordering strength of crystallographic preferred orientation data can be assessed in different ways, however, the appropriateness of the methodology used to do so can depend on the geometry of the distributions. Eigenvalue-based ordering evaluation methods, for example, may not be appropriate for data that comprise multiple, variably oriented distributions such as those commonly found in quartz *c*-axis crystallographic preferred orientations. In this study, we generate a series of artificial *c*-axis distributions using the R software environment and examine the correlations between different distribution geometries (i.e., the opening angle in a cross-girdled quartz *c*-axis pole figure) and the strengths of those distributions calculated using eigenvalue-based evaluation methods. This comparison demonstrates that larger pole figure opening angles correlate with decreasing distribution ordering strength. The same correlation does not exist when strength is evaluated using the $l^2$- norm of the estimated probability density function ($J_{PF}$) of the same data. The direct correlations between pole figure *c*-axis opening angles and ordering strength noted in the artificial distributions are also demonstrated in the evaluation of real-world data, though significant complications, perhaps related to the occurrence of non-quartz phases, variation in flow type and/or critically resolved stress, in the natural specimens can partially obfuscate the relationship. Regardless, given the potential effect of geometry on eigenvalue-based evaluation methods we recommend that the ordering strength of pole figure data be evaluated using $J_{PF}$.

Executive Editor:
**Janine Kavanagh**
Associate Editor:
**Dripta Dutta**
Technical Editor:
**Mohamed Gouiza**

Reviewers:
**Nicholas Hunter**
**Anonymous reviewer**

Submitted:
**28 September 2022**
Accepted:
**11 April 2023**
Published:
**11 May 2023**

## 1 Introduction

Quantifying finite strain is an aspiration of many geological studies, but in practice the extractable data often fall short of this goal. The relative differences in deformation intensity between specimens, however, are often easier to assess, typically require fewer assumptions (such as undeformed geometry) and, in many cases, can be nearly as insightful as measures of finite strain. Some studies have used the strength of ordering of crystal directions, or the crystallographic preferred orientations (CPO), for that purpose. The strength of a CPO has been used as a proxy for deformation intensity where stronger, more highly ordered CPOs have generally been interpreted to record greater strains (e.g. *Hansen et al.*, 2014; *Heilbronner and Tullis*, 2006) as long as dislocation creep is the governing deformation mechanism. Such interpretations are consistent with the results of deformation experiments (*Barnhoorn et al.*, 2004). In some works, the CPO strength of pole figures is quantified using eigenvalue-based methods (*Larson*, 2018; *Larson et al.*, 2017) such as cylindricity - B (*Vollmer*, 1990) and/or intensity – *I* (*Lisle*, 1985; *Mardia*, 1972). The orthogonality of the eigenvectors, however, means that the measures should not be applied to pole figures that consist of mixtures of two or more, variably oriented distributions (see *Mainprice et al.*, 2015), such as the crossed-girdle patterns frequently encountered in natural quartz c-axis pole figures. The problem with using eigenvalues for such distributions is that as the angle between the two girdles (the so-called opening angle) increases, the normalized S2 and S3 eigenvalues equalize and increase, effectively mimicking the expected result of less ordered pole figures. This fundamental aspect of eigenvalue-based evaluation metrics for spherical orientation data calls into question the results of past works that have used changes in B or *I* (for example) to infer associated variation in the strength of crossed girdle CPO pole figures and, accordingly, subsequent interpretations made based on those inferences.

An alternative method to quantify the strength of a sample of directions, such as in a pole figure, is to calculate the $l^2$- norm (Euclidean norm) of an estimated probability density function calculated for the spherical distribution of the orientation data (*Botev et al.*, 2010; *Kilian and Heilbronner*, 2017; *Mainprice et al.*, 2015). Following *Mainprice et al.* (2015), we refer to

*✉ kyle.larson@ubc.ca

this measure as $J_{PF}$.

Considering that the $l^2$- norm of a density function represents the Euclidean distance of that function from the origin, the $J_{PF}$ increases proportionally with the density expressed by a spherical orientation distribution. Because of this relationship, it is possible to use the $J_{PF}$ to estimate the degree of organization (or strength) expressed by a pole figure (Figure SI-1, Supporting Information). $J_{PF}$ of a uniform distribution is equal to 1, whereas that of a single point would result in an infinite value. Because the $J_{PF}$ is a function of the density of the pole orientations, it should not be biased by composite distributions such as crossed girdles like the eigenvalue-based methods. Note that $J_{PF}$ is similar to, but unique from $J^{ODF}$, as the latter refers to the l2-norm of the orientation distribution function (ODF) of crystal orientations and not vector data (*Mainprice et al.*, 2015). In the current contribution we are focused on quantifying CPO strength from pole figure data only. This focus, therefore, excludes other ODF-based distribution strength quantification parameters such as the M-index (*Skemer et al.*, 2005), R P factor (*Chateigner*, 2005), and texture entropy (*Schaeben et al.*, 1998). While comparison of such metrics is beyond the scope of the present work, it has been variably discussed in previously published studies (e.g. *Mainprice et al.*, 2015; *Skemer et al.*, 2005; *Wenk*, 2002).

To investigate the potential effects of changing pole figure geometries on various metrics of strength, we define a series of synthetic quartz *c*-axis distributions (Figure 1) with different opening angles representative of commonly observed distributions. The strengths of these pole figures were quantified using various eigenvalue-based methods and the $J_{PF}$. Analysis of the results demonstrates that the eigenvalue-based methods have a significant negative correlation between strength measure and opening angle.

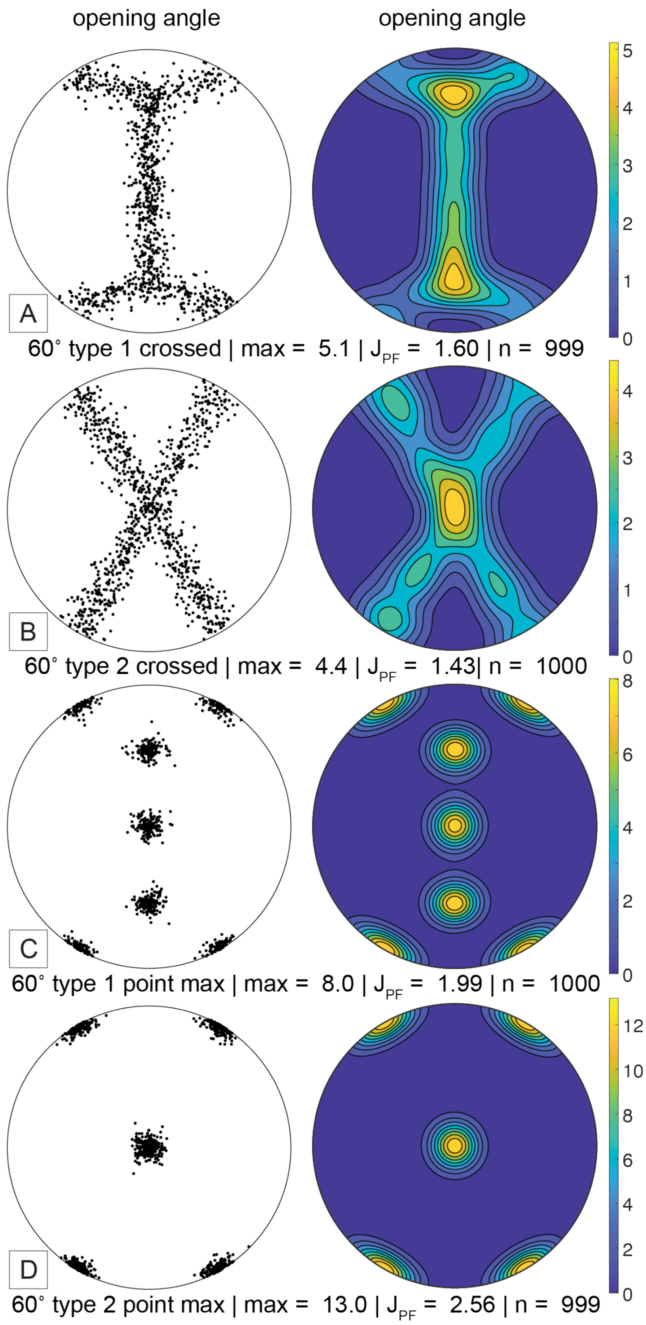


**Figure 1** – Representative examples of the modelled crystallographic preferred orientations (CPO) investigated. Contours follow the multiples of uniform density scale as in the colour scale. **A)** Type 1 crossed girdle; **B)** Type 2 crossed girdle; **C)** Type 1 crossed girdle approximated with point maxima distributions; **D)** Type 2 crossed girdle approximated with point maxima distributions.

## 2 Background

The field of spatial statistics has a rich and expansive history as it relates to geological sciences. Below we summarize some of the main works that have helped shape current practises as it relates to how spherical data have been collected and interpreted. As noted above, we are specifically restricting this to the assessment of axial, spherical data because of their common historical use in the literature to define qualitative strain gradients.

The use of the orientation tensors (*Fara and Scheidegger*, 1963; *Mardia*, 1972; *Scheidegger*, 1964, 1965; *Watson*, 1965, 1966) in the assessment of directional data has a long history in geosciences including formative works by *Woodcock* (1977) and *Woodcock and Naylor* (1983). In those studies, the authors outlined methods that can be used to evaluate both the shape of distributions of spherical data (clusters versus girdles) using a two axis logarithmic plot of the normalized eigenvalues, $S_1$, $S_2$ and $S_3$ of the orientation tensor (Woodcock, 1977) and the randomness of fabrics using the $S_1/S_3$ ratio (*Woodcock and Naylor*, 1983). *Woodcock* (1977) also defined the parameter C, equivalent to the natural logarithm of the $S_1/S_3$ ratio, as a measure of the strength of a preferred orientation. Critically, these early studies pointed out the limitations of eigenvalue-derived plots (as discussed above) related to high symmetry fabrics and specifically crossed girdle crystallographic preferred orientation data (*Woodcock*, 1977).

Subsequent studies have proposed alternative means of assessing the shape and characteristics of spherical data from the orientation tensor. *Lisle* (1985) proposed the Intensity, *I*, which was based on the uniformity statistic ($S_u$) of *Mardia* (1972), as a means to improve upon the $S_1/S_3$ test of randomness through accommodation of apparent differences in the ratio for cluster and girdle-type distributions and the fact that its distribution is not a simple function of sample size. Critically, distributions of similar geometry yield the same *I* value independent of sample size (*Lisle*, 1985). More recently, *Vollmer and SUNY New Paltz* (2020) suggested the 'fabric density index', D, an alternative to *I*, which, unlike *I*, ranges linearly between end member distribution geometries (0 = uniform, 0.5 = girdle, 1 = cluster).

*Vollmer* (1990) applied orientation tensor eigenvalues to structural domain analysis. In that work, Vollmer used the differences between the eigenvalues instead of the ratios to develop a triangular plot with axes corresponding to the fabric indexes P, R and G - point, random and girdle, respectively, that range between 0 and 1. Vollmer further defined a fourth index, cylindricity (B), the sum of P and G (equivalent to 1-R), which informs the ordering of the distribution independent of geometry (*Vollmer*, 1990). As *Woodcock* (1977) did previously, *Vollmer* (1990) pointed out that eigenvalue analysis is best employed for distributions with orthorhombic or unimodal axial symmetries. This same conclusion, specific to quartz *c*-axis orientations, was also reached by *Starkey* (1993).

The versatility and ease of use of the various eigenvalue-based methods has led to their recent usage to assess the strength of CPOs (e.g. *Graziani et al.*, 2020, 2022; *Hunter et al.*, 2018; *Larson*, 2018; *Larson et al.*, 2017; *Long et al.*, 2020, 2019; *Parsons et al.*, 2014; *Starnes et al.*, 2020). While some of those studies have compared eigenvalue-based results with those computed from the $J_{PF}$ (*Graziani et al.*, 2020; *Long et al.*, 2020) or other norm-based methods (*Hunter et al.*, 2018), most works have directly compared and interpreted the eigenvalue-based metrics, which resulted from crossed girdle pole figures. As noted above, however, the complex symmetries of crossed girdles means that such distributions may not be meaningfully assessed using the orientation tensor (*Mainprice et al.*, 2015; *Vollmer*, 1990; *Woodcock*, 1977).

## 3 Methods

To quantify the bias introduced by eigenvalue-based methods when estimating the relative strengths of axis distributions with different geometries, a series of synthetic axis distributions were generated. The R software environment *R Core Team* (2021) scripts written to generate the distributions are included in the Supplementary Data and summarily described below. The distributions investigated include different types of crossed girdles with variable opening angles or rotations (see Figure SI-2 for examples of each distribution, Supporting Information). Type 2 crossed girdle (Figure 1B; *Law et al.*, 2011, 2021, 2004; *Lister*, 1977) distributions were constructed using randomly generated numbers between 360 and 180 to define an azimuthal distribution that covered half a sphere (as projected in a lower hemisphere plot). Those data were effectively assigned a default plunge of 0°, placing them along the primitive. The plunges were then normally redistributed away from their original value with a standard deviation of 5°. These orientations were rotated 90 degrees counter-clockwise about a horizontal N-trending axis (all directions are given with respect to the primitive) to create a vertical single girdle and then further rotated about a vertical axis to achieve the appropriate girdle orientation. The same procedure was repeated to generate the second girdle to complete the distribution.

Type 1 crossed girdle distributions (Figure 1A; *Law et al.*, 2021, 2013; *Lister*, 1977; *Thigpen et al.*, 2010) were approximated by creating small circles with opposite opening directions through similar methods outlined above. The central septum was then calculated to intersect the small circles by generating a single girdle with a limited distribution based on the rake of the small circles in a vertical N-S plane. The number of points in the central septum and the small circle 'arms' was calculated based on their relative angular coverage on the sphere and a target total of ~1000 points.

The modified crossed girdle distribution geometries (Figure 1C, D) were developed based on multiple point distributions. These were constructed using a randomly generated azimuth between 1° and 360° and a plunge generated from a normal distribution around 90° with a standard deviation of 5°. Each point distribution was then rotated into its final position. The number of points was split evenly across the various maxima.

Finally, additional distributions were generated to investigate the potential effect of more diffuse data (Figure SI-3, Supporting Information) and the case where the c-axis distribution may be less dense toward the primitive (see pole figure CPOs in *Law et al.*, 2011). In the latter case, the point maxima approximations of Type 1 distributions were recalculated with half the density of points in the maxima at the primitive (Figure SI-4, Supporting Information).

All distributions were individually generated 5 times. The strength values are reported as the mean of those 5 iterations with uncertainties reported as the standard deviation. The MTEX toolbox (*Bachmann et al.*, 2010, https://mtex-toolbox.github.io/index.html) was used to generate contoured stereonet plots and calculate $J_{PF}$ (*Mainprice et al.*, 2015). For internal consistency, a de La Vallee-Poussin kernel with a half-width of 10° was used for density contours and $J_{PF}$ calculation for all distributions.

## 4 Results

Analysis of the modelled distributions shows that B, *I*, and D decrease with increasing opening angle of

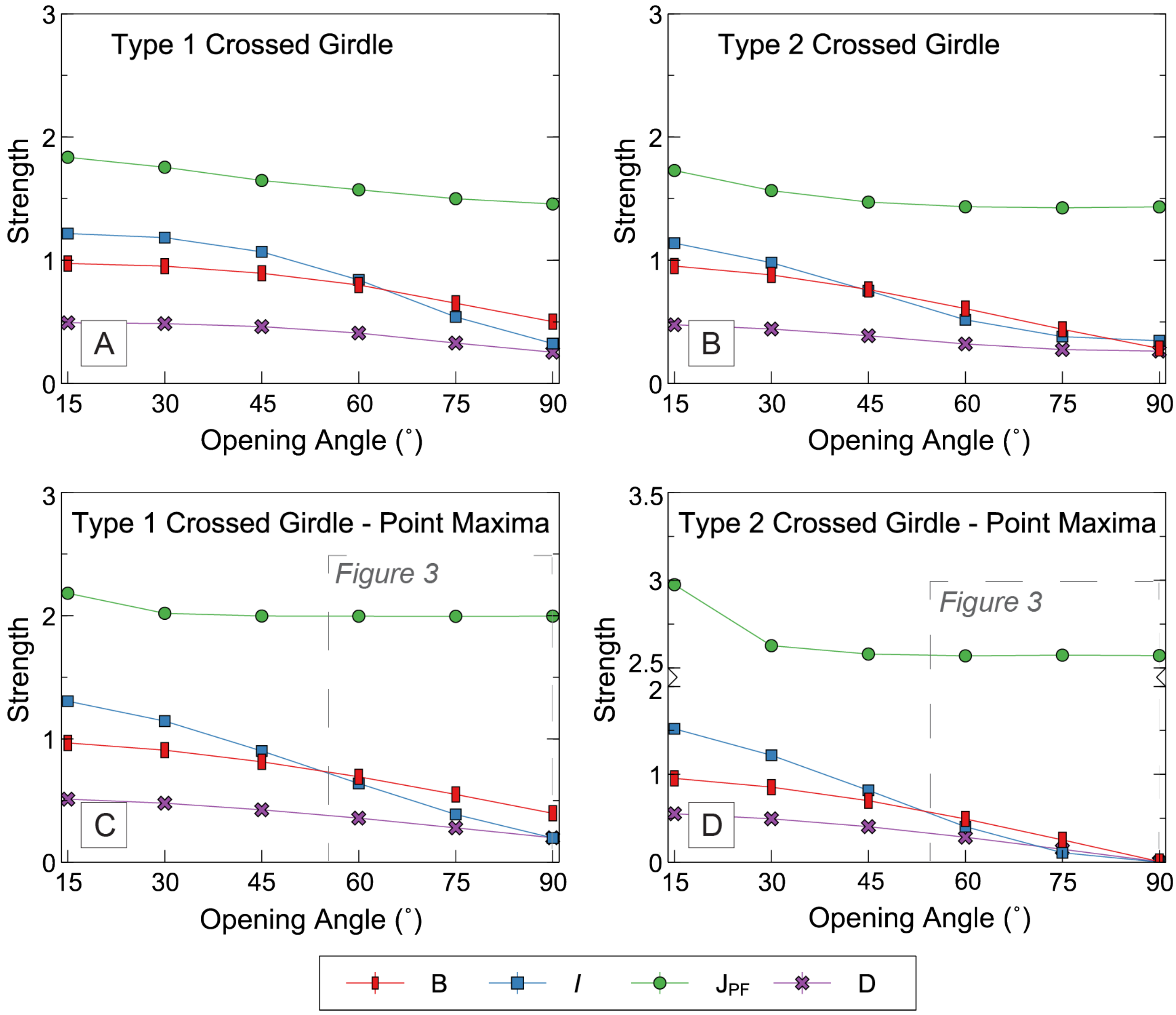


**Figure 2** – Summary diagram showing the effects of crystallographic preferred orientation (CPO) (single girdle and point maxima) and/or opening angle (crossed girdle) on different metrics of CPO strength. B = cylindricity; *I* = intensity; D = density; JPF = $l^2$- norm of the spherical density distribution.

the generated Type 1 and Type 2 crossed girdle distributions (Figure 2A, B). A similar, though less pronounced, trend is noted in the $J_{PF}$. We repeated the same analyses on the multimodal point distributions (Type 1 and Type 2 - style crossed "girdles") (Figure 2C, D). As before, B, *I* and D decrease with increasing opening angle. $J_{PF}$ of the multi-point distributions also decreases with increasing opening angle initially (< 30°), but is essentially unchanged at opening angles > 30°.

The point maxima-approximated Type 2 distributions with more diffuse data (i.e., point maxima with progressively larger variances in the normal distributions used to generate them), were also examined. The differences in the relationship between strength and opening angle between the variances, however, are minimal (Figure 3; Figure SI-3, Supporting Information). For the distributions generated with weaker peripheral maxima (Supplementary Figure 4), the relationship of increasing opening angle with decreasing distribution strength remains, but is diminished for B, *I* and D, while $J_{PF}$ is invariant (Figure 4).

## 5 Interpretations

The continuously decreasing B, *I*, and D with increasing opening angles in the generated Type 1 and Type 2 crossed girdle distributions of otherwise approximately identical geometries are consistent with the previously stated limitations of using the orientation tensor to represent complex geometries, and specifically pole figures represented by mixtures of distributions. The opening angle of quartz *c*-axis distributions has been correlated with temperature (*Faleiros et al.*, 2016; *Kruhl*, 1998; *Morgan and Law*, 2004). While this relationship may be debatable, and the authors of this manuscript may not agree on the justification of the relationship, it continues to be employed in many studies. Nevertheless, the range in opening angles explored in this work, 15° to 90°, would translate to a temperature range of ~ 150°C to ~ 660°C (using equations 1 and 2 of *Faleiros et al.*, 2016). Obviously, the above computations for opening angles > 90° will be identical to 180° minus the angle in question.

Due to the nature of quartz deformation, crossed girdle distributions with opening angles

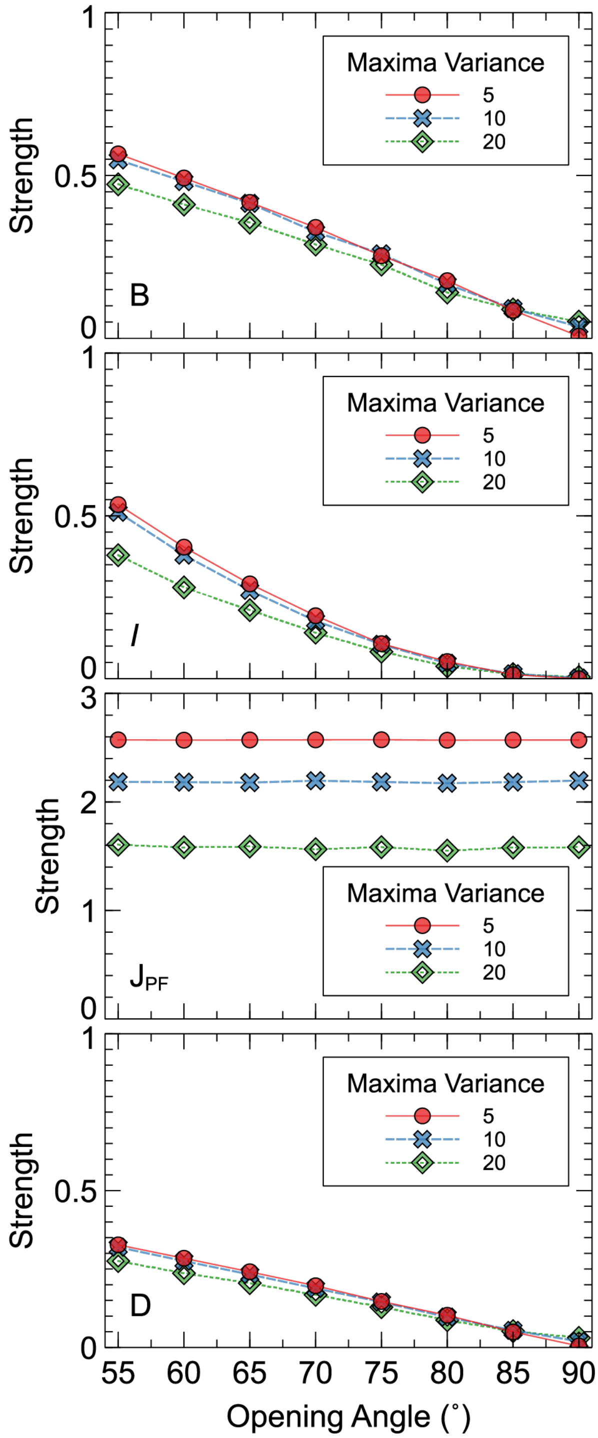


**Figure 3** – Distribution strength metrics for Type II maxima-based distributions generated with different variances around the point distribution maxima. B = cylindricity; *I* = intensity; D = density; JPF = $l^2$- norm of the spherical density distribution.

of ~ 55°–90° are common in the literature (see *Law*, 2014; *Law et al.*, 2004, 2011, 2013, 2021; *Morgan and Law*, 2004, and many other). As shown in Figure 5, even small 5° changes in opening angle between 55° and 90° can significantly affect the B, *I*, and D calculated for a distribution, whereas for the same range the $J_{PF}$ is essentially invariant. This result is critical as it shows the $J_{PF}$ is unaffected by changes across the opening angles most encountered in geological study.

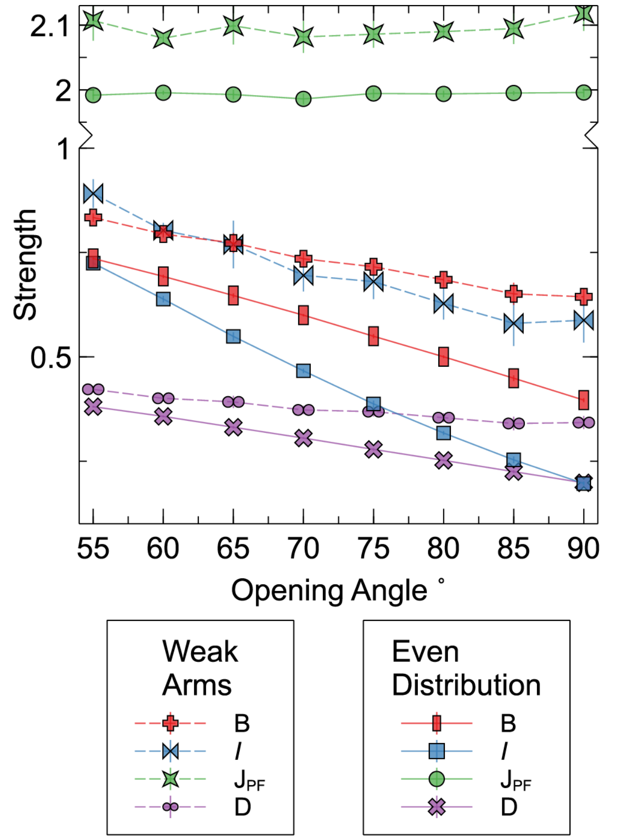


**Figure 4** – Quartz crystallographic preferred orientation (CPO)/fabric strength of Type 1 crossed girdles with different opening angles. The CPOs modelled using point maxima distributions in two different ways 1) as point maxima with an even distribution across all maxima and 2) as point maxima with reduced concentrations in the peripheral maxima ('weak arms'). B = cylindricity; *I* = intensity; D = density; JPF = $l^2$- norm of the spherical density distribution. See text for discussion.

## 6 Discussion

### 6.1 Study Limitations

The invariant nature of $J_{PF}$ applies for distributions that do not overlap, e.g., here between 30° and 90°. Where individual distributions overlap, as is the case for small distances separating distributions, sufficiently broad distributions, or overly large halfwidths used to assess the density, the norm of the density of the mixture must increase. The Type 2 synthetic distributions generated by simply adding and rotating two single girdle distributions (Figure 1B) overlap in the center. The associated increase in density can be further exacerbated by overlap along the primitive for increasingly small opening angles (< 30°; Figure 2; Figure SI-2, Supporting Information). The girdle geometries generated using point maxima distributions help avoid the central overlap but not overlap near the primitive for distributions separated by a small angle (i.e. < 30°; Figure SI-2, Supporting Information). Choosing a narrower kernel halfwidth to circumvent any overlap is not a solution as it will result in an overestimation of the density.

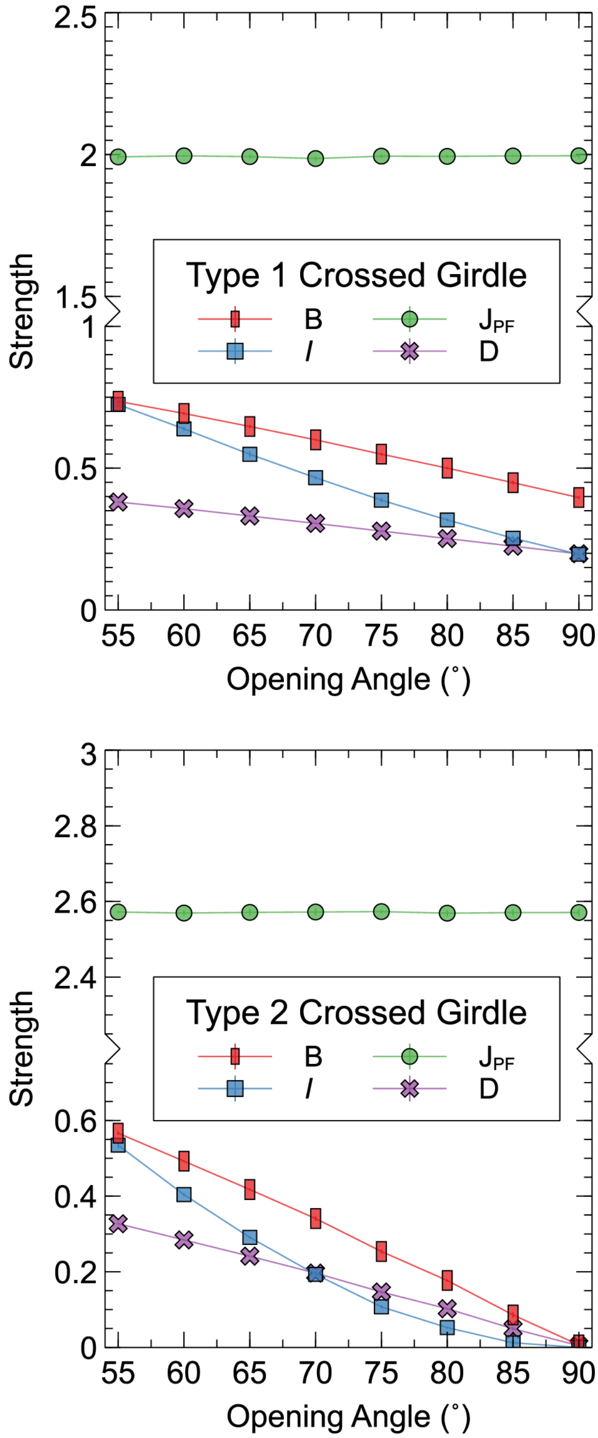


**Figure 5** – Distribution strength metrics with changing opening angle for Type 1 and Type 2 crossed girdle crystallographic preferred orientations as modelled with point maxima distributions. B = cylindricity; *I* = intensity; D = density; JPF = $I^2$- norm of the spherical density distribution.

## 6.2 Insights Based on the Analysis of Artificial Distributions

Regardless of the complications at smaller opening angles, when quantifying axial distributions in the typical range of interest of most studies, the $J_{PF}$ is essentially invariant making it the most appropriate measure of the strength of a distribution for pole figure CPO data. This can be visualized by plotting the difference in strength between different individual opening angles normalized to their maximum strength of that measure across the entire range of opening angles. Figure 6 shows that differences in B, I, and D for Type 1 crossed girdle distributions, calculated based on point maxima approximations (Figure 1) at 5° increments between 45 and 90°, do not

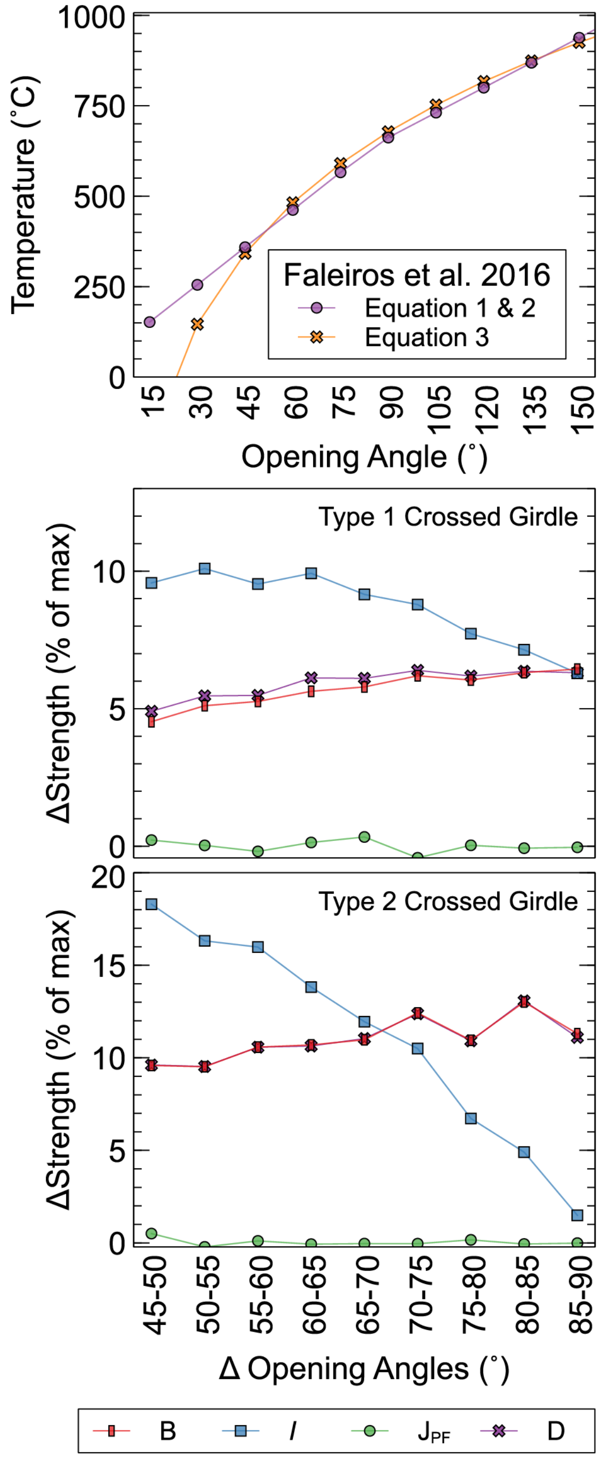


**Figure 6** – **Top**: Crystallographic preferred orientation (CPO) opening angle versus temperature as estimated from the equations of *Faleiros et al.* (2016). **Bottom**: The difference in strength calculated every 5° for opening angles between 45° and 90° for Type 1 and Type 2 crossed girdle CPO. The differences are normalized to the maximum CPO strength calculated for each strength parameter. B = cylindricity; *I* = intensity; D = density; $J_{PF}$ = $I^2$- norm of the spherical density distribution. See text for discussion.

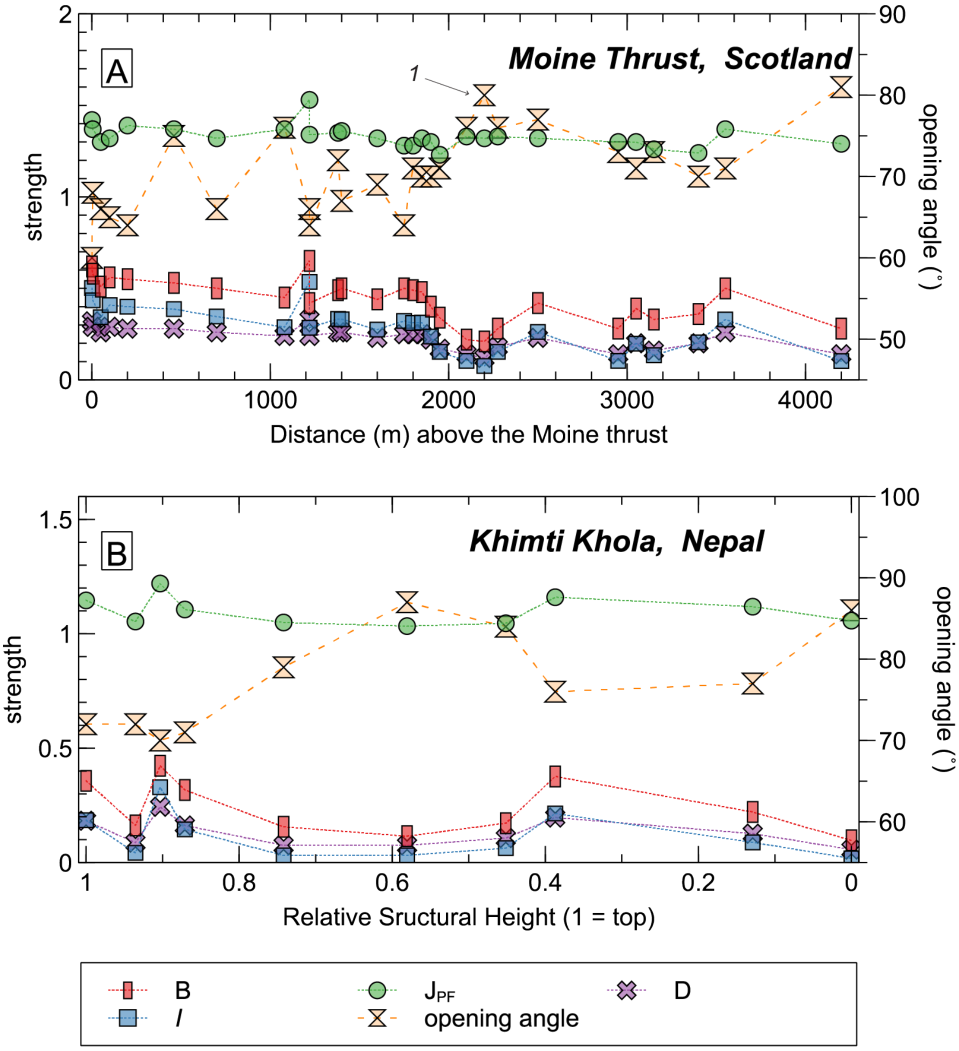


**Figure 7** – **A)** Quartz crystallographic preferred orientation (CPO) data (strengths and opening angles) published in *Law et al.* (2021) from plotted in structural position relative to the Moine thrust, Scotland. **B)** CPO data from *Larson* (2018) plotted as relative structural height with 1 being the top of the section from the Khimti Khola region of Nepal. B = cylindricity; I = intensity; D = density; $J_{PF}$ = $I^2$- norm of the spherical density distribution. See text for discussion.

vary much, consistent with their near-linear decrease with opening angle (Figure 5). The differences in distribution strengths calculated over the same intervals for Type 2 crossed girdles are larger, but broadly consistent for B and D, while they start out much higher and decrease nearly linearly for *I* to a minimum between 85° and 90° (Figure 6). Again, these patterns reflect those shown in Figure 5 where B and D decrease linearly with increasing opening angle and *I* decreases with a non-linear decay shape.

The difference in $J_{PF}$ calculated for 5° increments between 45° and 90° for both Type 1 and Type 2 crossed girdles is near zero and essentially invariant (Figure 5) demonstrating the lack of effect that opening angle has on the $J_{PF}$. Critically, the difference in $J_{PF}$ calculated is always significantly lower than B, *I*, and D. This relationship further shows that $J_{PF}$ should be used as the primary means to quantify the strength of CPOs.

## 6.3 Application to Real-World Data

While analysis of artificial distributions demonstrates the potential problems associated with relying on B, *I*, and D to quantify distribution strength when assessing crossed girdle pole figure CPOs, we can gain further insight by examining real-world data. To avoid potential complications of sampling across multiple deformation zones with complex deformation histories and widely varying lithologies, herein we focus on the expertly characterized, high-quality quartz CPO dataset from the immediate hanging wall of the Moine thrust, Scotland, published in *Law et al.* (2011).

Comparison of the spatial trends of the various strength parameters indicates that while the opening angle of crossed girdle distributions may affect B, *I*, and D, it may not be obvious in the overall patterns; the CPO strength profiles above the Moine thrust (Figure 5; *Law et al.*, 2021) appear similar for B, *I*, D, and $J_{PF}$. There are some notable exceptions, however, where changes in opening angle coincide with decoupling between the patterns of B, *I*, D, and $J_{PF}$. For example, at ~ 2100 m above the Moine thrust, the measured opening angle increases from 76° to 80° (Figure 7A; marked with a '1'). The $J_{PF}$ across those same specimens is essentially flat, however, there is a minor dip in B, *I*, and D.

If the strength data from the Moine thrust hanging wall are plotted against opening angle, however, the relationship of decreasing B, *I*, and D with increasing opening angle becomes apparent (Figure 8A). The Pearson linear coefficients (R2) calculated for B, *I*, and D range between 0.51 and 0.53, which indicates approximately half of the decrease in strength can be correlated with an increase in opening angle, whereas the same metric calculated for $J_{PF}$ is 0.09. The strong negative correlation between B, *I*, and D and opening angle, and lack of correlation between JPF and opening angle, is consistent with the expectations outlined from investigation of artificial distributions.

For comparison with the Moine hanging wall CPO data, the same style of investigation was applied to the data presented in *Larson* (2018) from the Khimti khola valley in central Nepal. Unlike the Moine data, the specimens from the Khimti khola are interpreted to record a spatially restricted, multi-deformational history. When plotted in relative structural position with opening angles, strength metrics appear to be coupled, behaving similarly across the field area (Figure 7B). When the strength data are plotted against opening angle alone, however, the expected negative relationship is observed (Figure 8B). In contrast to the Moine data, that same relationship is noted across all strength metrics including $J_{PF}$. The apparent departure from an expected 'flat' relationship between $J_{PF}$ and opening angle can be attributed to the multi-stage deformation history of the area. The specimens at the top of the structural section (>0.8 relative structural height; Figure 7B) are interpreted to record a late, high-strain deformation episode characterised by smaller quartz CPO opening angles and greater organization (*Larson*, 2018) resulting anomalously higher $J_{PF}$ that distort the relationship.

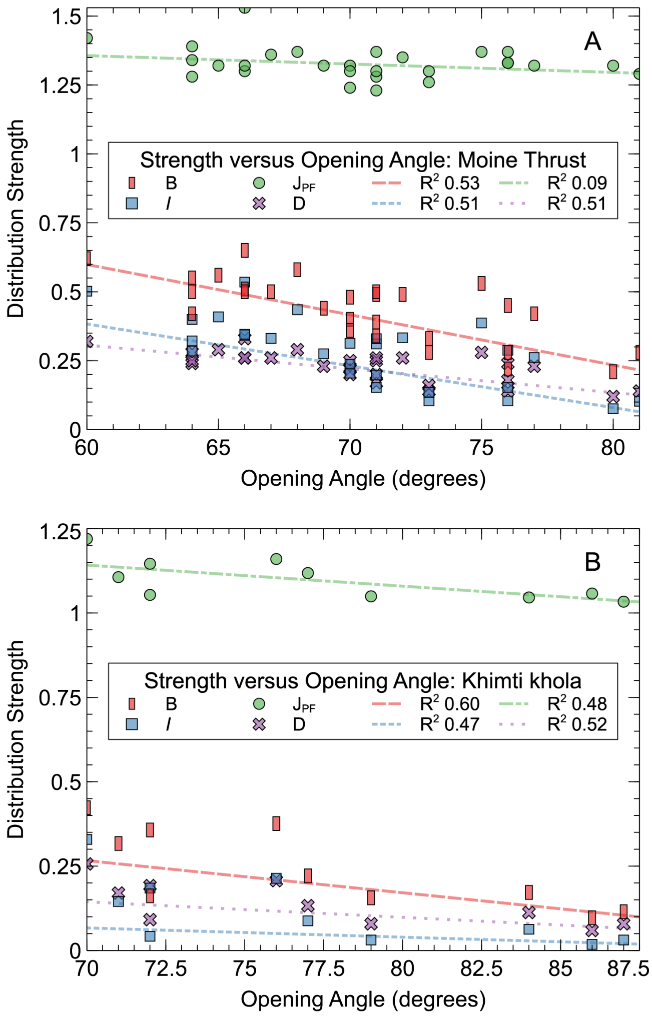


**Figure 8** – Distribution strength metrics plotted against opening angle for published data from the **A)** Moine thrust hanging all (*Law et al.*, 2021) and **B)** Khimti khola (*Larson*, 2018). The Pearson correlation coefficient (R2) for linear fits through each of the different metrics are reported. B = cylindricity; *I* = intensity; D = density; $J_{PF}$ = $l^2$- norm of the spherical density distribution.

Further complications in real-world datasets may be introduced by inter-sample variability. Changes in overall lithology, volume % quartz and other phases, the interconnected nature of quartz, finite strain, flow type and differential stress may all impact the development and strength of the CPO (*Graziani et al.*, 2020; *Herwegh et al.*, 2011; *Kilian et al.*, 2011; *Lister and Price*, 1978; *Lister and Williams*, 1979). Variable contributions from these factors may obfuscate the geometric relationship between eigenvalue-based strength measures and opening angles and indeed the limited studies that have published data from multiple parameters, including $J_{PF}$, from varying lithologies (*Graziani et al.*, 2020; *Long et al.*, 2020) show little difference in overall spatial strength patterns between methods.

# 7 Conclusions

Examination of synthetic distributions show that opening angle can have a significant effect on the calculated strength of crossed girdle pole figure CPOs using eigenvalue-based methods, B, *I*, and D, whereas strength determinations using the $l^2$- norm of the spherical density distribution ($J_{PF}$) are essentially unaffected. Those observations are supported by examination of real-world data from well-studied locations. Given the documented effect of different opening angles on distribution strength identified in artificial and natural data, it is recommended that the $J_{PF}$ be used in favour of eigenvalue-based strength determination methods when quantifying the strength of distributions of spherical axial data.

# Acknowledgements

Funding for this project was provided by a Natural Sciences and Engineering Research Council of Canada Discovery Grant and Canada Foundation for

Innovation John Evans Leadership Award to K. Larson. R. Law is thanked for sharing their dataset from the Moine thrust. Figures 2–6 were constructed using the free and open Veusz plotting package (https://veusz.github.io). Comments by F. Vollmer, N. Hunter and six anonymous reviewers helped improve various versions of this manuscript. D. Dutta and J. Kavanagh are thanked for careful and patient editorial handling.

## Author contributions

**K. Larson** conceived the study wrote the main text, prepared diagrams, and wrote the R script. **R. Graziani** edited the document, generated diagrams, and provided scientific interpretation. **R. Kilian** helped conceive the study, edit the text, provided scientific interpretation. **N. Piette-Lauzière** provided scientific interpretation and edited the manuscript.

## Data availability

R scripts for automating the generation of quartz CPO distribution data are hosted by the Open Science Foundation (https://osf.io/kh754/). The additional figures cited in the text can be found in the Supporting Information (https://tektonika.online/index.php/home/article/view/23/12).

## Competing interests

The authors declare no competing interests.

## Peer review

This publication was peer-reviewed by Nicholas Hunter and an anonymous reviewer. The full peer-review report can be found here: https://tektonika.online/index.php/home/article/view/23/13

## Copyright notice



## References

Bachmann, F., R. Hielscher, and H. Schaeben (2010), Texture analysis with MTEX – free and open source software toolbox, *Solid state phenomena*, *160*, 63–68, doi: 10.4028/www.scientific.net/ssp.160.63.

Barnhoorn, A., M. Bystricky, L. Burlini, and K. Kunze (2004), The role of recrystallisation on the deformation behaviour of calcite rocks: large strain torsion experiments on carrara marble, *Journal of Structural Geology*, *26*(5), 885–903, doi: 10.1016/j.jsg.2003.11.024.

Botev, Z. I., J. F. Grotowski, and D. P. Kroese (2010), Kernel density estimation via diffusion, *The Annals of Statistics*, *38*(5), 2916–2957, doi: 10.1214/10-AOS799.

Chateigner, D. (2005), Reliability criteria in quantitative texture analysis with experimental and simulated orientation distributions, *Journal of applied crystallography*, *38*(4), 603–611, doi: 10.1107/s0021889805013695.

Faleiros, F. M., R. Moraes, M. Pavan, and G. A. C. Campanha (2016), A new empirical calibration of the quartz *c*-axis fabric opening-angle deformation thermometer, *Tectonophysics*, *671*, 173–182, doi: 10.1016/j.tecto.2016.01.014.

Fara, H. D., and A. E. Scheidegger (1963), An eigenvalue method for the statistical evaluation of fault plane solutions of earthquakes, *Bulletin of the Seismological Society of America*, *53*(4), 811–816, doi: 10.1785/bssa0530040811.

Graziani, R., K. P. Larson, and M. Soret (2020), The effect of hydrous mineral content on competitive strain localization mechanisms in felsic granulites, *Journal of Structural Geology*, *134*(104015), 104,015, doi: 10.1016/j.jsg.2020.104015.

Graziani, R., K. Larson, M. Smit, J. M. Cottle, J. Lamming, and N. Piette-Lauzière (2022), Modern style nappe stacking in the paleoproterozoic lower crust: An example from the snowbird tectonic zone, canadian shield, *Precambrian research*, *380*(106817), 106,817, doi: 10.1016/j.precamres.2022.106817.

Hansen, L. N., Y.-H. Zhao, M. E. Zimmerman, and D. L. Kohlstedt (2014), Protracted fabric evolution in olivine: Implications for the relationship among strain, crystallographic fabric, and seismic anisotropy, *Earth and planetary science letters*, *387*, 157–168, doi: 10.1016/j.epsl.2013.11.009.

Heilbronner, R., and J. Tullis (2006), Evolution of c axis pole figures and grain size during dynamic recrystallization: Results from experimentally sheared quartzite, *Journal of geophysical research*, *111*(B10), doi: 10.1029/2005jb004194.

Herwegh, M., J. Linckens, A. Ebert, A. Berger, and S. H. Brodhag (2011), The role of second phases for controlling microstructural evolution in polymineralic rocks: A review, *Journal of Structural Geology*, *33*(12), 1728–1750, doi: 10.1016/j.jsg.2011.08.011.

Hunter, N. J. R., R. F. Weinberg, C. J. L. Wilson, V. Luzin, and S. Misra (2018), Microscopic anatomy of a "hot-on-cold" shear zone: Insights from quartzites of the main central thrust in the alaknanda region (garhwal himalaya), *GSA Bulletin*, *130*(9-10), 1519–1539, doi: 10.1130/B31797.1.

Kilian, R., and R. Heilbronner (2017), Analysis of crystallographic preferred orientations of experimentally deformed black hills quartzite, *Solid earth*, *8*(5), 1095–1117, doi: 10.5194/se-8-1095-2017.

Kilian, R., R. Heilbronner, and H. Stünitz (2011), Quartz microstructures and crystallographic preferred orientation: Which shear sense do they indicate?, *Journal of Structural Geology*, *33*(10), 1446–1466, doi: 10.1016/j.jsg.2011.08.005.

Kruhl, J. H. (1998), Prism- and basal-plane parallel subgrain boundaries in quartz: a microstructural geothermobarometer: Reply, *Journal of Metamorphic Geology*, *16*, 142–146.

Larson, K., J. Cottle, G. Lederer, and S. M. Rai (2017), Defining shear zone boundaries using fabric intensity gradients: An example from the east-central nepal himalaya, *Geosphere*, *13*(3), 771–781, doi: 10.1130/ges01373.1.

Larson, K. P. (2018), Refining the structural framework of the khimti khola region, east-central nepal himalaya, using quartz textures and c-axis fabrics, *Journal of Structural Geology*, *107*, 142–152, doi: 10.1016/j.jsg.2017.12.014.

Law, R. D. (2014), Deformation thermometry based on quartz *c*-axis fabrics and recrystallization microstructures: A review, *Journal of Structural Geology*, *66*, 129–161, doi: 10.1016/j.jsg.2014.05.023.

Law, R. D., M. P. Searle, and R. L. Simpson (2004), Strain, deformation temperatures and vorticity of flow at the top of the greater himalayan slab, everest massif, tibet, *Journal of the Geological Society*, *161*(2), 305–320, doi: 10.1144/0016-764903-047.

Law, R. D., M. J. Jessup, M. P. Searle, M. K. Francsis, D. J. Waters, and J. M. Cottle (2011), Telescoping of isotherms beneath the south tibetan detachment system, mount everest massif, *Journal of Structural Geology*, *33*(11), 1569–1594, doi: 10.1016/j.jsg.2011.09.004.

Law, R. D., D. W. Stahr, III, M. K. Francsis, K. T. Ashley, B. Grasemann, and T. Ahmad (2013), Deformation temperatures and flow vorticities near the base of the greater himalayan series, sutlej valley and shimla klippe, NW india, *Journal of Structural Geology*, *54*, 21–53, doi: 10.1016/j.jsg.2013.05.009.

Law, R. D., J. R. Thigpen, S. E. Mazza, C. A. Mako, M. Krabbendam, B. M. Spencer, K. T. Ashley, R. A. Strachan, and E. F. Davis (2021), Tectonic transport directions, shear senses and deformation temperatures indicated by quartz c-axis fabrics and microstructures in a NW-SE transect across the moine and sgurr beag thrust sheets, caledonian orogen of northern scotland, *Geosciences*, *11*(10), 411, doi: 10.3390/geosciences11100411.

Lisle, R. J. (1985), The use of the orientation tensor for the description and statistical testing of fabrics, *Journal of Structural Geology*, *7*(1), 115–117, doi: 10.1016/0191-8141(85)90119-1.

Lister, G. S. (1977), Discussion: Crossed-girdle c-axis fabrics in quartzites plastically deformed by plane strain and progressive simple shear, *Tectonophysics*, *39*(1-3), 51–54, doi: 10.1016/0040-1951(77)90087-7.

Lister, G. S., and G. P. Price (1978), Fabric development in a quartz-feldspar mylonite, *Tectonophysics*, *49*(1-2), 37–78, doi: 10.1016/0040-1951(78)90097-5.

Lister, G. S., and P. F. Williams (1979), Fabric development in shear zones: theoretical controls and observed phenomena, *Journal of Structural Geology*, *1*(4), 283–297, doi: 10.1016/0191-8141(79)90003-8.

Long, S. P., C. L. Mullady, J. K. Starnes, S. M. Gordon, K. P. Larson, L. S. Pianowski, R. B. Miller, and E. Soignard (2019), A structural model for the south tibetan detachment system in northwestern bhutan from integration of temperature, fabric, strain, and kinematic data, *Lithosphere*, *11*(4), 465–487, doi: 10.1130/l1049.1.

Long, S. P., M. J. Kohn, B. C. Kerswell, J. K. Starnes, K. P. Larson, N. R. Blackford, and E. Soignard (2020), Thermometry and microstructural analysis imply protracted extensional exhumation of the tso morari UHP nappe, northwestern himalaya: Implications for models of UHP exhumation, *Tectonics*, *39*(12), 663, doi: 10.1029/2020tc006482.

Mainprice, D., F. Bachmann, R. Hielscher, and H. Schaeben (2015), Descriptive tools for the analysis of texture projects with large datasets using MTEX: strength, symmetry and components, *Geological Society, London, Special Publications*, *409*(1), 251–271, doi: 10.1144/SP409.8.

Mardia, K. V. (1972), 9 - INFERENCE PROBLEMS ON THE SPHERE, in *Statistics of Directional Data*, edited by K. V. Mardia, pp. 249–283, Academic Press, doi: 10.1016/B978-0-12-471150-1.50015-7.

Morgan, S. S., and R. D. Law (2004), Unusual transition in quartzite dislocation creep regimes and crystal slip systems in the aureole of the eureka Valley–Joshua Flat–Beer creek pluton, california: a case for anhydrous conditions created by decarbonation reactions, *Tectonophysics*, *384*(1-4), 209–231, doi: 10.1016/j.tecto.2004.03.016.

Parsons, A. J., R. J. Phillips, G. E. Lloyd, M. P. Searle, and R. D. Law (2014), Quantified vertical strain profile through the greater himalayan sequence, Annapurna-Dhaulagiri himalaya, central nepal, *Journal of Himalayan Earth sciences*, *Abstract29th Himalaya-Karakoram-Tibet Workshop*, 126–127.

R Core Team (2021), R: A language and environment for statistical computing. R foundation for statistical computing.

Schaeben, H., H. Siemes, and J. J. Fundenberger (1998), The ill-posedness of the inverse problem of texture goniometry: The variation width of feasible orientation density functions revisited, *Journal of applied crystallography*, *31*(2), 136–148, doi: 10.1107/s002188989700825x.

Scheidegger, A. E. (1964), The tectonic stress and tectonic motion direction in europe and western asia as calculated from earthquake fault plane solutions, *Bulletin of the Seismological Society of America*, *54*(5A), 1519–1528, doi: 10.1785/bssa05405a1519.

Scheidegger, A. E. (1965), ON THE STATISTICS OF THE ORIENTATION OF BEDDING PLANES, *U.S. Geological Survey Professional Paper*, *525*, 164.

Skemer, P., I. Katayama, Z. Jiang, and S.-I. Karato (2005), The misorientation index: Development of a new method for calculating the strength of lattice-preferred orientation, *Tectonophysics*, *411*(1-4), 157–167, doi: 10.1016/j.tecto.2005.08.023.

Starkey, J. (1993), The analysis of three-dimensional orientation data, *Canadian journal of earth sciences*, *30*(7), 1355–1362, doi: 10.1139/e93-116.

Starnes, J. K., S. P. Long, S. M. Gordon, J. Zhang, and E. Soignard (2020), Using quartz fabric intensity parameters to delineate strain patterns across the himalayan main central thrust, *Journal of Structural Geology*, *131*(103941), 103,941, doi: 10.1016/j.jsg.2019.103941.

Thigpen, J. R., R. D. Law, G. E. Lloyd, and S. J. Brown (2010), Deformation temperatures, vorticity of flow, and strain in the moine thrust zone and moine nappe: Reassessing the tectonic evolution of the scandian foreland–hinterland transition zone, *Journal of Structural Geology*, *32*(7), 920–940, doi: 10.1016/j.jsg.2010.05.001.

Vollmer, F. W. (1990), An application of eigenvalue methods to structural domain analysis, *Geological Society of America bulletin*, *102*(6), 786–791, doi: 10.1130/0016-7606(1990)102<0786:aaoemt>2.3.co;2.

Vollmer, F. W., and SUNY New Paltz (2020), Representing progressive fabric paths on a triangular plot using a fabric density index and crystal axes eigenvector barycenters, in *Geological Society of America Abstracts with Programs 52(6)*, 358862, Geological Society of America, Montreal, QC, doi: 10.1130/abs/2020am-358862.

Watson, G. S. (1965), Equatorial distributions on a sphere, *Biometrika*, *52*(1/2), 193–201, doi: 10.2307/2333824.

Watson, G. S. (1966), The statistics of orientation data, *The Journal of geology*, *74*(5, Part 2), 786–797, doi: 10.1086/627211.

Wenk, H.-R. (2002), 10. texture and anisotropy, in *Plastic Deformation of Minerals and Rocks*, edited by S.-I. Karato and H.-R. Wenk, pp. 291–330, De Gruyter, Berlin, Boston.

Woodcock, N. H. (1977), Specification of fabric shapes using an eigenvalue method, *GSA Bulletin*, *88*(9), 1231–1236, doi: 10.1130/0016-7606(1977)88<1231:SOFSUA>2.0.CO;2.

Woodcock, N. H., and M. A. Naylor (1983), Randomness testing in three-dimensional orientation data, *Journal of Structural Geology*, *5*(5), 539–548, doi: 10.1016/0191-8141(83)90058-5.